

Potential window of stable stoichiometry of solid-state electrolyte materials

Tobias Binninger,^{*,†,‡} Aris Marcolongo,^{†,‡} Valéry Weber,[†] and Teodoro Laino[†]

[†]*IBM Research – Zurich, Säumerstrasse 4, CH-8803 Rüschlikon, Switzerland*

[‡]*Contributed equally to this work.*

E-mail: tbi@zurich.ibm.com

Abstract

We present a novel method to estimate the stability potential window of solid-state electrolyte (SSE) materials in all-solid-state batteries. We consider exchange processes of both electrons and mobile ion species (Li^+ , Na^+ , ...) at the interface between the SSE and the respective electrode in order to compute the chemical potential of the mobile species. The latter reveals a discontinuity as a function of the mobile species stoichiometry. We connect this jump in the chemical potential to the potential window of stable stoichiometry of the SSE, which can be inexpensively computed, ideal for integration into SSE material screening workflows. The results of the novel method are compared for a selection of relevant Li- and Na-SSE materials against the results of state-of-the-art methods, namely the HOMO–LUMO method and the grand potential phase diagram method. The novel method is complementary to and represents a bridge between the two latter methods. Furthermore, we rationalize how even small changes of the SSE stoichiometry can lead to severe self-discharge of an all-solid-state battery resulting in fading of battery charge over time.

Keywords

all-solid-state battery, solid-state electrolyte, electrochemical stability potential window, SSE stoichiometry, battery self-discharge

Introduction

Solid-state electrolyte (SSE) materials, i.e. materials that provide ionic but no electronic conductivity, are key components of all-solid-state batteries, which are regarded as promising candidates for next generation batteries. State-of-the-art Li-ion batteries are based on liquid organic electrolytes, which are flammable and furthermore thermodynamically unstable against the low-potential electrode, e.g. metallic Li. Their operation is possible only due to the formation of a passivating layer between the electrode and the liquid electrolyte, termed the solid electrolyte interphase (SEI) layer.^{1,2} In comparison to liquid electrolytes, many SSE materials offer superior stability against reduction and oxidation. Nevertheless, only few SSE materials provide true thermodynamic stability against the corresponding metallic anode^{3,4} and, therefore, interfacial stability between the electrode and the solid-state electrolyte is a focus topic in current all-solid-state battery research.^{5,6} For many SSE materials, a passivating interphase layer forms between the metallic low-potential electrode and the SSE,^{3,5-7} which consists of SSE decomposition products, similar to the SEI layer in liquid electrolyte Li-ion batteries. Although such a “metal–solid electrolyte interphase (MSEI) layer”⁷ can render an all-solid-state battery meta-stable due to passivation and also provide a certain ionic conductivity to sustain battery operation, the battery performance will be deteriorated because of the reduced ionic conductivity of the interphase layer. The same conclusion holds for passivating interphase layers between the SSE and the high-potential electrode.⁴ Thus, in order for all-solid-state batteries to unfold their full potential, an intrinsic thermodynamic stability of the SSE against both electrodes is desirable. These interface stability properties are directly described by the electrochemical stability potential window of an SSE material,

which is defined as the set of potentials vs. a given reference electrode where no reduction or oxidation of the SSE material occurs.

From a computational point of view, the positions of the electronic HOMO and LUMO states, i.e. the valence and conduction band edges, provide an approximate estimate of the stability potential window⁸⁻¹⁰ via the electronic band gap. In this approach, the electrode in contact with the SSE acts as “electron reservoir” and only electron exchange between electrode and SSE is considered. The “HOMO–LUMO method” allows for a rather quick estimation of the width of the stability potential window. However, the absolute position with respect to a reference electrode is very difficult to assess. In fact, this methodology includes neither interface dipole effects,⁹ nor ion exchange between electrode and SSE.

As an alternative, but more complex method, the grand potential phase diagram of the SSE can be computed at various values of the chemical potential of the mobile species,^{3,10,11} taking into account all possible decomposition products. The processes considered within this approach are written in terms of direct chemical reactions between the SSE and the respective electrode material under exchange of neutral atoms of the mobile species, i.e. of both the cations (Li^+ , Na^+ , ...) and their associated electrons. In contrast to the HOMO–LUMO method, the grand potential phase diagram method provides the absolute position of the stability potential window with respect to a certain reference, however at the expense of a rather large effort required for the identification and computational characterization of all relevant decomposition reactions for each SSE material. Possible amorphous decomposition products are very difficult to identify and model computationally within the grand potential phase diagram.

In the present work, we propose a novel method to compute the stability properties of an SSE material in terms of its potential window of stable stoichiometry. Similar to the grand potential phase diagram method, we consider reactions originating from the exchange of neutral atoms of the mobile species between electrode and SSE. However, whereas the phase diagram method takes into account processes that result in major decomposition of the SSE

into products with very different structure and composition, our approach considers processes that result in small changes of the SSE stoichiometry by generating or filling vacancies within the SSE structure. These processes enable a direct computation of the chemical potential of the mobile species as a function of the SSE stoichiometry, which directly yields the potential window of stable stoichiometry of an SSE.

A closely connected, defect chemistry-derived perspective on SSE stability has recently been used to investigate the instability of $\text{Li}_4\text{P}_2\text{S}_6$ SSE against metallic Li,¹² however without relating this perspective to the general framework of electrochemical stability and the computation of the stability potential window of general SSE materials.

The novel approach not only provides a complementary method for the computation of the SSE stability potential window, but we will show that it forms a bridge between the HOMO–LUMO method and the grand potential phase diagram method, providing additional fundamental insight and justification related to these state-of-the-art methods. Furthermore, we argue how the changes in SSE stoichiometry associated with the Li (or Na, ...) exchange result in an intrinsic self-discharge instability of the all-solid-state battery.

Theory

Fundamental processes of A-exchange

In the following, we indicate with A, where $A = \text{Li}, \text{Na}, \dots$, the mobile species within an SSE material. Further, we denote as $A_n\text{M}$ the most stable composition for a unit cell of an SSE material, where the precise meaning of “most stable” is further specified below. Inside an all-solid-state battery, the SSE material $A_n\text{M}$ is in contact with both the anode (low potential) and the cathode (high potential) electrode. During battery operation, exchange of A^+ between SSE and electrode materials occurs, as required for the function of the battery. However, in principle also exchange of (neutral) A is possible, for which reason the thermodynamic stability properties must be considered from the perspective of an A-grand

canonical ensemble.¹⁰ The most basic A-exchange processes between SSE and the electrode materials correspond to insertion of additional A into the SSE or, vice versa, extraction of A from the SSE, respectively:



where ϵ is understood to be small compared to n .

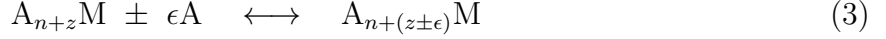
There exists a qualitative difference between adding A to and extracting A from the most stable composition $A_n M$. In general, $A_n M$ corresponds to a stoichiometry where all constituting ions formally are in a favorable electronic closed shell configuration. The electrons of added A populate the LUMO states of $A_n M$, whereas the electrons of extracted A are removed from the HOMO states. SSE materials are electronic isolators with a band gap $E_{A_n M}^{\text{LUMO}} - E_{A_n M}^{\text{HOMO}} > 0$, thus leading to different energetic behavior of the two processes (1) and (2).

The critical difference between these processes and the exchange of A^+ between SSE and electrode materials during normal battery operation is the fact that processes (1) and (2) lead to a change of the oxidation state of other species in the M-matrix. These processes represent redox-reactions between SSE and the respective electrode material, and are not required for the function of the battery. As shown later, if these processes occur, the all-solid-state battery can become inherently unstable due to self-discharge.

Potential window of stable stoichiometry

Processes (1) and (2) were written as deviations from the most stable composition $A_n M$, leading to a general composition $A_{n+z} M$. When $z \neq 0$ there is no need to distinguish the

two processes of adding and subtracting A and the overall A-exchange reactions read:



Reaction (3) defines an equilibrium potential Φ_{eq} vs. a given reference potential Φ_{ref} . In an A-ion battery context, the latter is generally taken to be the equilibrium potential of the A-metal oxidation process $A \leftrightarrow A^+ + e^-$. The equilibrium potential Φ_{eq} of reaction (3) is a function of the stoichiometry deviation z and can be expressed in terms of the corresponding Gibbs free energy of reaction via the Nernst equation:

$$\Phi_{\text{eq}} = -\frac{\Delta G}{e(\pm\epsilon)} = -\frac{1}{e(\pm\epsilon)} \left(G_{A_{n+(z\pm\epsilon)}M} - G_{A_{n+z}M} - (\pm\epsilon)G_A \right) \quad (4)$$

$$= -\frac{1}{e} \left(\frac{G_{A_{n+(z\pm\epsilon)}M} - G_{A_{n+z}M}}{\pm\epsilon} - G_A \right) \quad (5)$$

$$= -\frac{1}{e} \left(\mu_{\text{SSE}}^A(z) - \mu_A^A \right) \quad (6)$$

Here, $\mu_A^A = G_A$ is the chemical potential of A-metal, i.e. its Gibbs free energy per atom, and $\mu_{\text{SSE}}^A(z)$ corresponds to the chemical potential of species A for the SSE composition $A_{n+z}M$,

$$\mu_{\text{SSE}}^A(z) = \lim_{\epsilon \rightarrow 0} \frac{G_{A_{n+(z+\epsilon)}M} - G_{A_{n+z}M}}{\epsilon} = \frac{dG}{dz} \quad (7)$$

which is equal to the derivative of the Gibbs free energy $G(z) := G_{A_{n+z}M}$ as a function of the deviation z from the most stable stoichiometry.

For $z > 0$, the surplus of A introduces additional electrons which must occupy states close to or within the conduction band. Vice versa, for $z < 0$, electrons are withdrawn from the valence band. Therefore, the most stable stoichiometry n separates two distinct energetic manifolds with the consequence that the chemical potential μ_{SSE}^A has a discontinuity at $z = 0$ with $\lim_{z \rightarrow 0^+} \mu_{\text{SSE}}^A$ being strictly larger than $\lim_{z \rightarrow 0^-} \mu_{\text{SSE}}^A$.

Based on this rationale, we derive an approximate expression of the Gibbs free energy

$G(z)$ for $|z| \ll 1$, i.e. for small deviations from the most stable composition. For this purpose, the Gibbs free energy (per unit cell) $G = U + pV - TS$ is first approximated by $G = E_0 - TS_{\text{conf}}$, in which only the energy E_0 at $T = 0$ K and the configurational entropy S_{conf} of A-site occupation are taken into account. Within this most basic approximation, other contributions like the pV term, the vibrational zero-point energy, the vibrational internal energy, and the vibrational entropy are neglected, which is well justified if an error of ± 0.1 V is acceptable on the calculated stability potential window. If higher accuracy is required, such corrections can be included in the computational method in a straightforward manner, of course at a higher computational cost.

For $|z| \ll 1$, the energy of adding one A to the general composition $A_{n+z}M$ is approximately constant, i.e. $E_0 \approx E_0^0 + \Delta E_0^{+/-} z$, for $z \gtrless 0$, respectively. Here, as argued above, it is taken into account that this energy $\Delta E_0^{+/-}$ of adding A is discontinuous at $z = 0$, resulting in two different constant values $\Delta E_0^+ > \Delta E_0^-$ for $z \gtrless 0$, respectively.

Within this simplified 1-type A-site model, it is assumed that all A-sites are energetically equivalent (cf. Supporting Information for a more general 2-type A-site model). Assuming a total number $n + m$ of A-sites, either occupied or unoccupied, per unit cell of the material $A_{n+z}M$, the configuration entropy S_{conf} results from the combinatorics of filling $n + z$ out of a total of $n + m$ sites:

$$S_{\text{conf}} = \frac{1}{N_c} k_B \log \left(\frac{N_c (n + m)}{N_c (n + z)} \right) \quad (8)$$

$$\approx k_B ((n + m) \log(n + m) - (n + z) \log(n + z) - (m - z) \log(m - z)) \quad (9)$$

where k_B is the Boltzmann constant and where Stirling's approximation was applied, because the total number N_c of unit cells in the entire crystal is very large. Thus, we obtain

$$\mu_{\text{SSE}}^{\text{A}}(z) = \Delta E_0^{+/-} - k_B T \log \left(\frac{n + m}{n + z} - 1 \right) \quad (10)$$

where the $+/-$ refer to $z > 0$ and $z < 0$, respectively, and together with Relation (4)

$$\Phi_{\text{eq}} = \Phi_{\text{I/II}} + \frac{k_B T}{e} \log \left(\frac{n+m}{n+z} - 1 \right) \quad (11)$$

where

$$\Phi_{\text{I/II}} := -(\Delta E_0^{+/-} - \mu_A^A)/e \quad (12)$$

again for $z > 0$ and $z < 0$, respectively, and with $\Phi_{\text{I}} < \Phi_{\text{II}}$ because $\Delta E_0^+ > \Delta E_0^-$.

Vice versa, for a given electrode potential Φ , the equilibrium stoichiometry deviation z of the SSE in contact with the respective electrode is obtained by resolving Equation (11) with $\Phi_{\text{eq}} = \Phi$:

$$z = \begin{cases} \frac{(n+m)}{1+\exp((\Phi-\Phi_{\text{I}})/\gamma)} - n & , \Phi < \Phi_{\text{I}} + \delta \\ 0 & , \Phi_{\text{I}} + \delta \leq \Phi \leq \Phi_{\text{II}} + \delta \\ \frac{(n+m)}{1+\exp((\Phi-\Phi_{\text{II}})/\gamma)} - n & , \Phi_{\text{II}} + \delta < \Phi \end{cases} \quad (13)$$

where $\gamma = \frac{k_B T}{e}$ and $\delta = \gamma \log(m/n)$. In relevant cases, this shift δ can be neglected: for a practical SSE material, the number of occupied and unoccupied A-sites will be of the same order of magnitude. Even for $m/n = 10^{\pm 1}$, it follows $|\delta| \approx 2\gamma$ with $\gamma = 0.025 \text{ V}$ for $T \approx 300 \text{ K}$. Accounting for an acceptable error of $\pm 0.1 \text{ V}$, we will neglect the shift δ in the following.

Figure 1 plots the deviation z as a function of the electrode potential Φ as described by Equation (13) for an arbitrary choice of $n = 1$, $m = 1$, $\Phi_{\text{I/II}} = \mp 0.5 \text{ V}$, and for $\gamma = 0.025 \text{ V}$ corresponding to $T \approx 300 \text{ K}$. The stoichiometry dramatically changes in two step steps below/above $\Phi_{\text{I/II}}$, the width of each step being defined by the scale γ . The step below Φ_{I} corresponds to SSE reduction, whereas the step above Φ_{II} corresponds to SSE oxidation. At

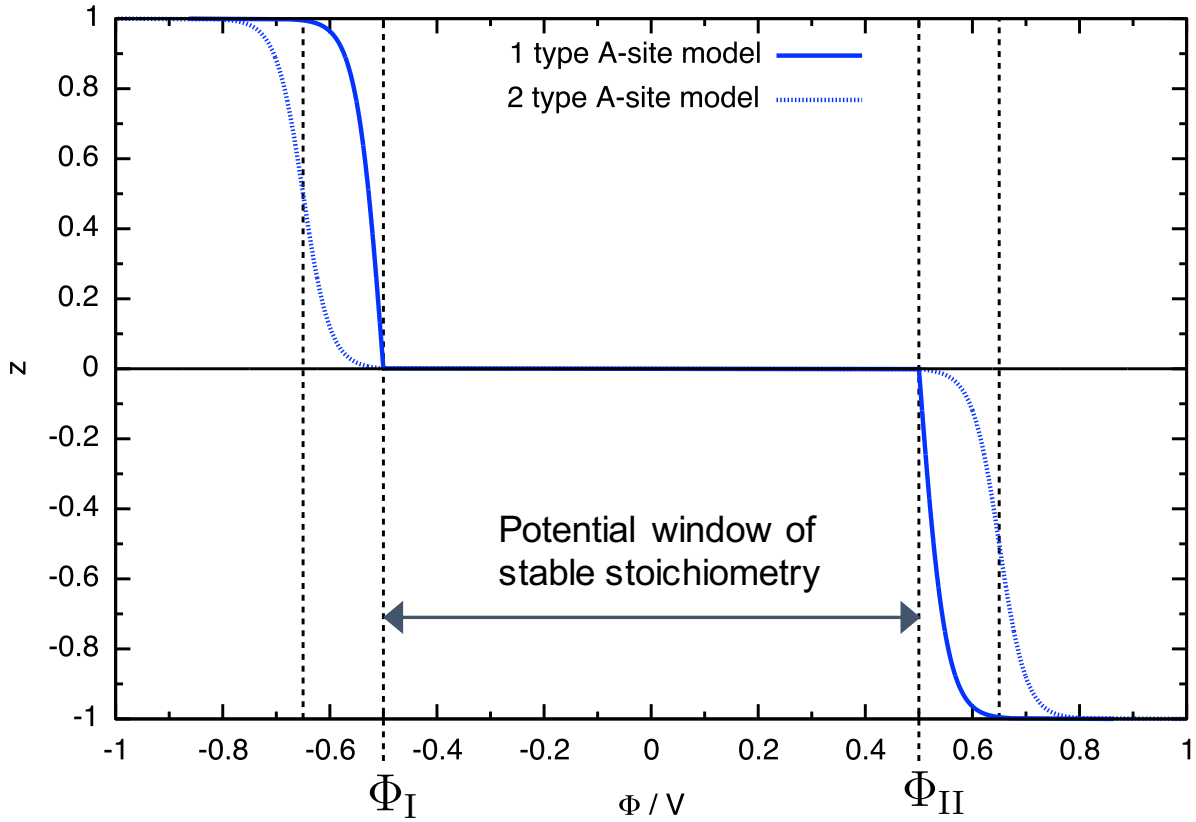


Figure 1: The stoichiometry deviation z in the general SSE material $A_{n+z}M$ as a function of the potential Φ as derived from the model in the limit $|z| \ll 1$. Also plotted is the result of an extended model taking into account two energetically different types of A-sites, cf. Supporting Information.

potentials in between these limits, i.e. $\Phi_I \leq \Phi \leq \Phi_{II}$, the stoichiometry deviation is equal to zero, $z = 0$. These potentials form a potential window of stable stoichiometry, where the SSE is stable in the composition A_nM and the valencies of all SSE constituent ions remain constant.

Within the present model we assume that all $n + m$ A-sites within the SSE material A_nM are energetically equivalent, i.e. every distribution of the n A over the $n + m$ sites has the same energy. However, in general, there will be energetic variations between different distributions. In the Supporting Information we present an extended model which takes into account two different classes of A sites in the material A_nM : one class of n occupied ground-state sites, and another class of m vacant excited-state sites. Such a 2-type A-site

model mimics the situation e.g. for doped SSE materials where dopant-induced trapping effects lead to an energetic splitting of A-sites. The resulting z vs. Φ is also plotted in Figure 1 for identical parameters plus an energetic splitting of 0.3 eV between ground- and excited-state sites. The essential features are preserved in the extended model, but the steep edges at $\Phi_{I/II}$ are smoothed and the turning points of both steps are shifted according to the energetic splitting between the two A-site classes.

Relevance of the potential window of stable stoichiometry

It appears intuitive that major SSE decomposition due to A-exchange with the electrode materials, as considered within the grand potential phase diagram method, requires a stronger thermodynamic driving-force than the filling or generation of single A-vacancies in the preserved SSE structure according to Processes (1) and (2). The additional insertion or extraction of A can be considered as a first step, whereas major decomposition reactions set in after the stoichiometry deviation z reaches critical values that render the SSE structure unstable as a whole. Therefore, we expect that the limits Φ_I and Φ_{II} , cf. Equation (12), of the potential window of stable stoichiometry also represent good estimates for those potentials at which major decomposition reactions set in, because just below Φ_I and above Φ_{II} the stoichiometry deviation z strongly changes within a narrow potential range so that critical values of z are quickly reached. We will critically discuss this intuitive picture further below in light of the computational results.

Diffusion self-discharge of all-solid-state batteries. The potential window of stable stoichiometry has further fundamental importance in the stability assessment of an SSE material when applied in an all-solid-state battery. Firstly, even small stoichiometry changes of the SSE material can significantly increase its electronic conductivity. This becomes clear from a doping perspective: Addition of A to the material introduces electrons into the (previously empty) conduction band. Similarly, extraction of A generates electron holes in

the valence band. Of course, the extent of electronic conductivity induced by A-stoichiometry changes is strongly material-specific, because it critically depends on whether the additional electronic charge carriers occupy mobile states within the conduction or valence band, or whether they get trapped by states lying deeply within the band-gap.

Secondly, as shown in the following, small stoichiometry changes of the SSE material can, in fact, result in a severe intrinsic self-discharge of an all-solid-state battery. In order to explain this diffusion-driven self-discharge mechanism, we consider an entire all-solid-state battery where the SSE is in contact with the anode on one side and with the cathode on the other side. At both contact interfaces, the SSE will equilibrate with the respective electrode material according to Processes (1) and (2). This is equivalent to the SSE stoichiometry deviation z attaining values defined by the respective electrode potential according to Equation (13). If both the anode potential Φ_A and the cathode potential Φ_C lie inside the potential window $[\Phi_I, \Phi_{II}]$, the SSE stoichiometry deviation z is equal to zero everywhere and the SSE material is stable. If, however, $\Phi_A < \Phi_I$ and/or $\Phi_C > \Phi_{II}$, the SSE stoichiometry deviation z_A at the anode contact interface will be different from the value z_C at the cathode contact interface, with $z_A > z_C$. Thus, an A-stoichiometry gradient is generated inside the SSE material, which, in turn, triggers A-diffusion from the anode side to the cathode side. Since no external flow of electrons is required for this mechanism, it will proceed also under open-circuit conditions, and, therefore, result in self-discharge of the all-solid-state battery.

The critical question is the speed of the resulting diffusion self-discharge for a given all-solid-state battery configuration. In order to estimate at which levels of $\Delta z = z_A - z_C$ the diffusion self-discharge becomes significant, we consider an all-solid-state battery with an SSE layer thickness of $d_{\text{SSE}} = 100 \mu\text{m}$, and an SSE bulk conductivity of $\sigma = 10^{-3} \text{ S/cm}$. Applying the Nernst-Einstein equation for the diffusion coefficient of A within the SSE, $D = (k_B T / n_A q_A^2) \sigma$, with a typical mobile ion density $n_A = 10^{21} \text{ cm}^{-3}$ and charge $q_A = e$, we estimate $D \approx 10^{-7} \text{ cm}^2 \text{ s}^{-1}$. For such values, a small relative SSE stoichiometry gradient of $\Delta z / n = 0.05$ between the anode interface and the cathode interface translates into a gradient

of mobile ion density $\Delta n_A = n_A (\Delta z/n) = 5 \times 10^{19} \text{ cm}^{-3}$. Then, according to Fick's law of diffusion, the self-discharge diffusion flux of A is approx. $|j_A| \approx D\Delta n_A/d_{\text{SSE}} \approx 5 \times 10^{14} \text{ cm}^{-2}\text{s}^{-1}$, which is equivalent to an electrical self-discharge current of $|j_{el}| = e|j_A| \approx 0.08 \text{ mA cm}^{-2}$. A typical Li-ion battery contains approx. 20 mg cm^{-2} of active cathode material with specific capacitance of approx. 150 mAh/g , yielding an area-specific battery capacitance of approx. 3 mAh cm^{-2} . Such a battery would be entirely self-discharged within approx. 1.5 days. Even for $D = 10^{-8} \text{ cm}^2\text{s}^{-1}$, a complete self-discharge time of approx. two weeks is obtained, rendering such an all-solid-state battery useless especially for long-term and seasonal electricity storage applications.

In such estimate, it must be taken into account that this *chemical* diffusion of A resulting from a stoichiometry gradient is different from the *ionic* diffusion of A^+ , which is coupled to the ionic conductivity by the Nernst-Einstein equation. However, chemical diffusion of A can be regarded as a parallel diffusion of both A^+ and electrons e^- .¹³ If the electronic mobility is large, the chemical diffusion coefficient will be essentially equal to the ionic one. The SSE material in its most stable stoichiometry is an electronic isolator, but, as soon as the A-stoichiometry deviates, mobile electronic charge carriers are generated. Therefore, the ionic diffusion coefficient can provide a good estimate of the relevant chemical diffusion coefficient in the non-stoichiometric composition region of the SSE material. Because synthesis of a non-stoichiometric SSE material appears difficult, an experimental determination of the chemical diffusion coefficient in non-stoichiometric SSE materials must be challenging. However, it has been reported that e.g. NASICON with an excess of Na reveals improved ionic conductivity,¹⁴ which is an experimental indication that fast chemical diffusion of Na is possible in such materials. Further theoretical studies must be devoted in the future to elucidate the differences between chemical vs. ionic diffusion in non-stoichiometric SSE materials.

Computational Method

Basic equations. A great advantage of the evaluation of SSE material stability in terms of its potential window of stable stoichiometry is the facile computational implementation. This becomes very attractive for material screening purposes, where the computation of the potential window of stable stoichiometry can be performed as a first screening step, so that a large amount of unstable materials are filtered out before expensive simulations of the ion conductivity are performed.

The evaluation of the potential window of stable stoichiometry only requires the calculation of the energies of adding and of removing one A to/from the most stable stoichiometry A_nM :

$$\Delta E_0^+ = E_{A_{n+1}M} - E_{A_nM} \quad (14)$$

$$\Delta E_0^- = E_{A_nM} - E_{A_{n-1}M} \quad (15)$$

In order to fix the reference potential, also the chemical potential of A-metal μ_A^A must be computed, which is equal to the Gibbs free energy per atom $\mu_A^A = G_A = U + pV - TS$. Again, if an error of ± 0.1 V is acceptable, the pV and the entropy terms can be neglected and the internal energy U can be approximated by the energy per atom E_A^A at $T = 0$ K without vibrational contributions, resulting in $\mu_A^A \approx E_A^A$. Of course, if higher accuracy is desired, the vibrational contribution to the internal energy and to the entropy can be taken into account in a straightforward manner. Finally, the lower and upper limits of the potential window of stable stoichiometry are obtained from Equation (12),

$$\Phi_I \approx -\frac{1}{e}(E_{A_{n+1}M} - E_{A_nM} - E_A^A) \quad (16)$$

$$\Phi_{II} \approx -\frac{1}{e}(E_{A_nM} - E_{A_{n-1}M} - E_A^A) \quad (17)$$

Computational details. The novel method was tested for a set of important SSE materials. We investigated the Li-ion conductors $\text{Li}_{10}\text{GeP}_2\text{S}_{12}$ (LGPS), O-doped $\text{Li}_2\text{PO}_2\text{N}$ (LIPON), $\text{Li}_7\text{La}_3\text{Zr}_2\text{O}_{12}$ (LLZO), $\text{Li}_{0.33}\text{La}_{0.56}\text{TiO}_3$ (LLTO), $\text{Li}_{1.33}\text{Al}_{0.33}\text{Ti}_{1.67}(\text{PO}_4)_3$ (LATP), and $\text{Li}_{3.5}\text{Zn}_{0.25}\text{GeO}_4$ (LISICON), as well as the binary MSEI compounds Li_2O , Li_2S , Li_3N , Li_3P , and LiF , all of which had already been studied by the grand potential phase diagram method.³ Since the precise LIPON composition $\text{Li}_2\text{PO}_2\text{N}$ does not contain accessible Li-vacancies,¹⁵ one Li-vacancy was generated in the computational supercell by replacing one nitrogen by an oxygen atom, resulting in a precise composition of $\text{Li}_{1.9375}\text{PO}_{2.0625}\text{N}_{0.9375}$. Furthermore, we also investigated the NASICON Na-ion conductor $\text{Na}_3\text{Zr}_2\text{Si}_2\text{PO}_{12}$.

We used the following workflow to compute the potential window of stable stoichiometry:

1. Get .cif-file including site occupancies.
2. Construct supercells with random configurations according to the occupancies for each of the A-stoichiometries N , $N+1$, and $N-1$, whereby N refers to the total number of A per supercell according to the most stable SSE stoichiometry specified in the .cif-file.
3. Compute the energy of each configuration after optimization of cell and coordinates.
4. Take the lowest energy configuration of each of the A-numbers N , $N+1$, and $N-1$. In order to take into account thermal activation of higher energy configurations, also the thermal average, $\sum_i E_i \exp(-E_i/(k_B T))/Z$ with $Z = \sum_i \exp(-E_i/(k_B T))$, of the energies of different configurations can be used. However, since the thermal excitation energy $k_B T$ is of the order of few 10 meV at relevant temperatures, the influence of using the thermal average compared to the lowest energy configuration is minor.
5. Apply Equations (16) and (17).

The energies per atom E_A^A of metallic Li and Na were computed only once from optimized structures. For all materials, the supercells were large enough to keep the changes in A-

stoichiometry small due to adding or extracting one A. Table 1 summarizes the origin of .cif-files and the corresponding crystal structures, as well as the supercell compositions used for the computations. For each material, depending on the combinatorial degree of freedom, we considered approximately 20–30 different random configurations of the N, N+1, and N-1 A-stoichiometries.

Table 1: Details regarding input .cif-files, structures, and supercells for the investigated materials.

Material	Origin of .cif	Structure	Supercell composition
LGPS	ICSD-188886 Ref. ¹⁶	Tetragonal	$\text{Li}_{80}\text{Ge}_8\text{P}_{16}\text{S}_{96}$
LIPON	Ref. ¹⁵	Orthorhombic	$\text{Li}_{31}\text{P}_{16}\text{O}_{32}(\text{N}_{15}\text{O})$
LLZO	ICSD-422259 Ref. ¹⁷	Cubic	$\text{Li}_{56}\text{La}_{24}\text{Zr}_{16}\text{O}_{96}$
LLTO	ICSD-82671 Ref. ¹⁸	Tetragonal	$\text{Li}_{12}\text{La}_{20}\text{Ti}_{36}\text{O}_{108}$
LATP	ICSD-253240 Ref. ¹⁹	Hexagonal	$\text{Li}_8\text{Al}_2\text{Ti}_{10}\text{P}_{18}\text{O}_{72}$
LISICON	ICSD-100169 Ref. ²⁰	Orthorhombic	$\text{Li}_{56}\text{Zn}_4\text{Ge}_{16}\text{O}_{64}$
Li_2O	COD-1010064 Ref. ²¹	Cubic	$\text{Li}_{64}\text{O}_{32}$
Li_2S	COD-1010874 Ref. ²²	Cubic	$\text{Li}_{64}\text{S}_{32}$
Li_3N	COD-1544904 Ref. ²³	Hexagonal	$\text{Li}_{108}\text{N}_{36}$
Li_3P	COD-1010290 Ref. ²⁴	Hexagonal	$\text{Li}_{144}\text{P}_{48}$
LiF	COD-1010990 Ref. ²⁵	Cubic	$\text{Li}_{108}\text{F}_{108}$
NASICON	COD-1529809 Ref. ²⁶	Hexagonal	$\text{Na}_{18}\text{Zr}_{12}\text{Si}_{12}\text{P}_6\text{O}_{72}$

Computations were performed at the level of density functional theory (DFT) implemented in the Quantum ESPRESSO software package.²⁷ The generalized gradient approximation (GGA) of the exchange-correlation functional in PBE form²⁸ was used along with ONCV pseudopotentials.^{29,30} An energy cutoff of 80 Ryd was used for the plane wave basis functions. Due to the usage of supercells, k -point sampling was restricted to the Γ -point and the convergence of the results was confirmed by certain computations using a 2x2x2 k -point mesh.

Results and Discussion

Table 2 summarizes the computed values for the limits $\Phi_{\text{I/II}}$ of the potential window of stable stoichiometry for all investigated SSE materials and Figure 2 presents results in comparison

with the corresponding stability potential windows as published in Ref,³ which were computed with the grand potential phase diagram method using DFT with PBE functional as in the present work. In order to check the influence of other DFT parameters and the different software environment, we re-computed the results from the grand potential phase diagram method for LGPS and LIPON confirming the published values³ with a very good agreement within approx. 0.1 V.

Table 2: Lower and upper limits $\Phi_{\text{I/II}}$ and corresponding widths $\Delta\Phi$ of the potential window of stable stoichiometry for all investigated SSE materials. Potential limits are given vs. the reference potential of A-metal oxidation, whereby A corresponds to Li for all Li-SSE materials and to Na for NASICON. Also given are the electronic Fermi level differences ΔE_{F} between the systems with A-stoichiometries N+1 and N, and the electronic HOMO–LUMO band gap values ΔE_{BG} for the most stable A-stoichiometry N.

Material	$\Phi_{\text{I}} / V_{\text{vs. A}}$	$\Phi_{\text{II}} / V_{\text{vs. A}}$	$\Delta\Phi / \text{V}$	$\Delta E_{\text{F}} / \text{eV}$	$\Delta E_{\text{BG}} / \text{eV}$
LGPS	1.19	3.66	2.47	1.99	2.00
LIPON	0.41	4.47	4.06	2.17	5.43
LLZO	-0.45	3.37	3.82	3.97	4.33
LLTO	1.76	4.09	2.33	2.40	2.38
LATP	0.70	3.31	2.61	2.47	2.48
LISICON	-0.10	3.56	3.66	3.53	3.55
Li ₂ O	–	3.45	–	–	–
Li ₂ S	–	3.38	–	–	–
Li ₃ N	–	1.05	–	–	–
Li ₃ P	–	1.77	–	–	–
LiF	–	6.84	–	–	–
NASICON	-0.36	4.38	4.74	4.31	4.60

Taking into account an error $\gtrsim 0.5$ V on redox potentials computed at DFT GGA level³¹ and a similar error on the results of the grand potential phase diagram method computed at the same level of theory, agreement between the results from the two different methods is found for the lower stability potential limits of LGPS, LIPON, LLZO, and LLTO and for the upper potential limits of LLZO, LLTO, and LISICON.

Larger upper stability potential limits result from the novel method for LGPS and LIPON and smaller lower stability potential limits for LATP and LISICON. In these cases, the grand potential phase diagram method provides stricter stability limits than the novel method of

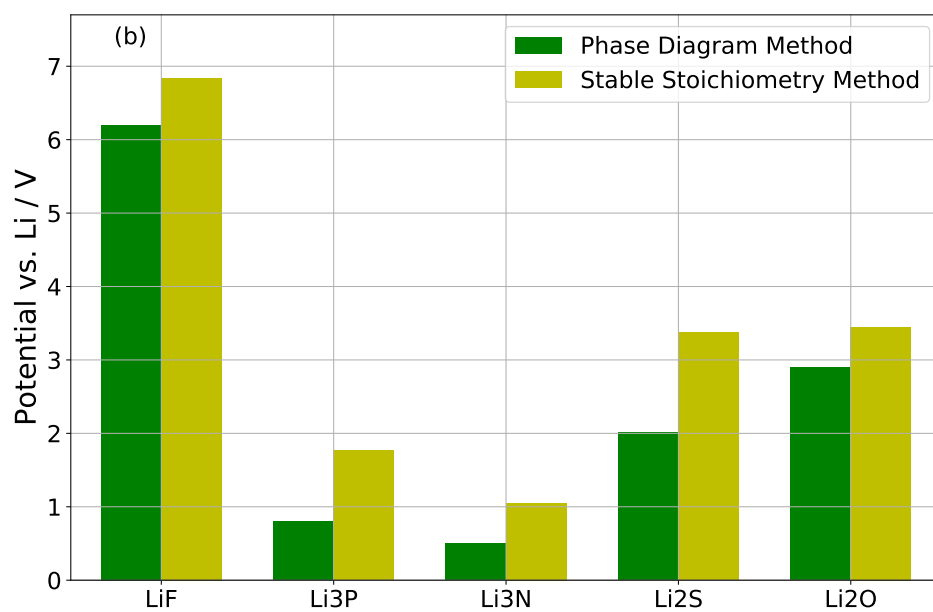
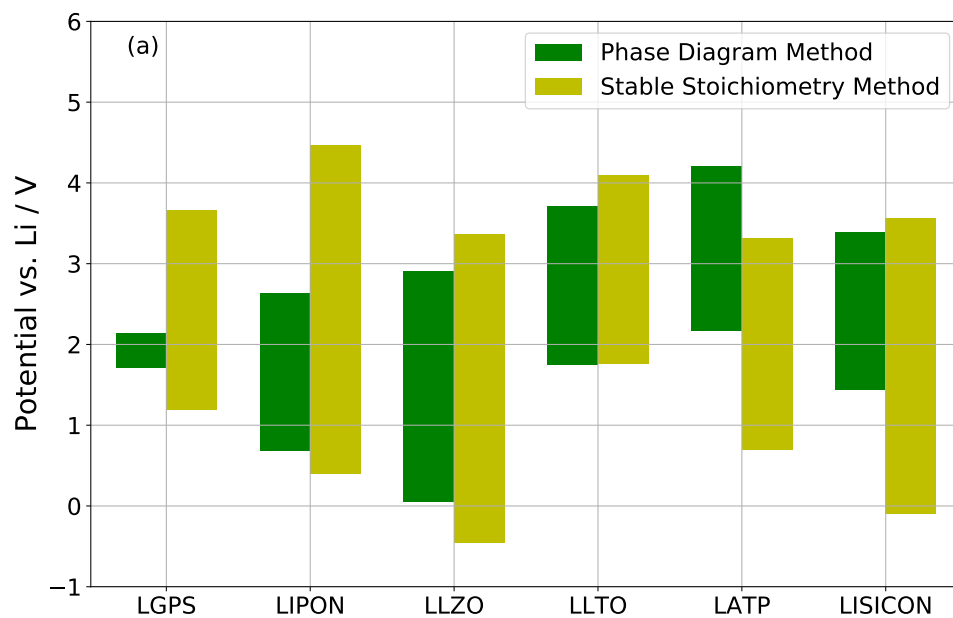


Figure 2: Potential windows of stable stoichiometry for various Li-SSE materials (a) and binary Li-MSEI compounds (b) computed with the novel method in comparison with the results published in Ref³ computed with the grand potential phase diagram method.

stable SSE stoichiometry. However, the novel method yields a smaller, and thus stricter upper stability potential limit for LATP.

We conclude that the two methods stand in a complementary relation. The decomposition reactions considered in the grand potential phase diagram method represent the limit of large stoichiometric and structural changes, whereas the novel method represents the limit of infinitesimal stoichiometry changes with a preserved crystal structure. As explained above, even such small SSE stoichiometry changes open up a major loss channel in an all-solid-state battery via diffusion self-discharge. Therefore, the corresponding potential window of stable stoichiometry is fundamental for the battery stability and, thus, complementary to the stability potential window resulting from the grand potential phase diagram. Accordingly, the overall stability potential window is given by the intersection of both potential windows.

Considering infinitesimal changes as more favorable than major decomposition reactions, one expects that the potential window of stable stoichiometry is stricter than the stability potential window according to the grand potential phase diagram method. Such a situation was found for the upper stability potential limit of LATP. However, in some other cases the opposite was obtained, i.e. the grand potential phase diagram method provided stricter limits than the novel method of stable stoichiometry. In these cases, surprisingly, major decomposition reactions are thermodynamically more favourable than infinitesimal stoichiometry changes. However, even in such a situation, the addition/extraction of single A atoms to/from the SSE could represent the first mechanistic step, which would result in a kinetic hindrance of the decomposition reaction up to the stable stoichiometry potential limit. In light of the larger upper stability potential limits obtained for LGPS and LIPON from the novel method, this kinetic mechanism could explain the experimentally apparent higher stability against electrochemical oxidation of LGPS³² and LIPON³³ in comparison with the computed upper stability potential limits from the grand potential phase diagram method.³

Turning to the results for Na-SSE, a negative value of the lower potential limit $\Phi_{\text{I}} =$

$-0.36 V_{\text{vs. Na}}$ was obtained for NASICON, cf. Table 2. This result serves as an indication of stoichiometric stability of NASICON against a Na metal electrode (corresponding to $0 V_{\text{vs. Na}}$). However, taking into account an error of $\approx 0.5 V$, the possibility of a weak instability against Na metal should be considered. Also experimental studies do not reveal a conclusive answer to the question whether NASICON is thermodynamically stable³⁴ or unstable³⁵ against metallic sodium.

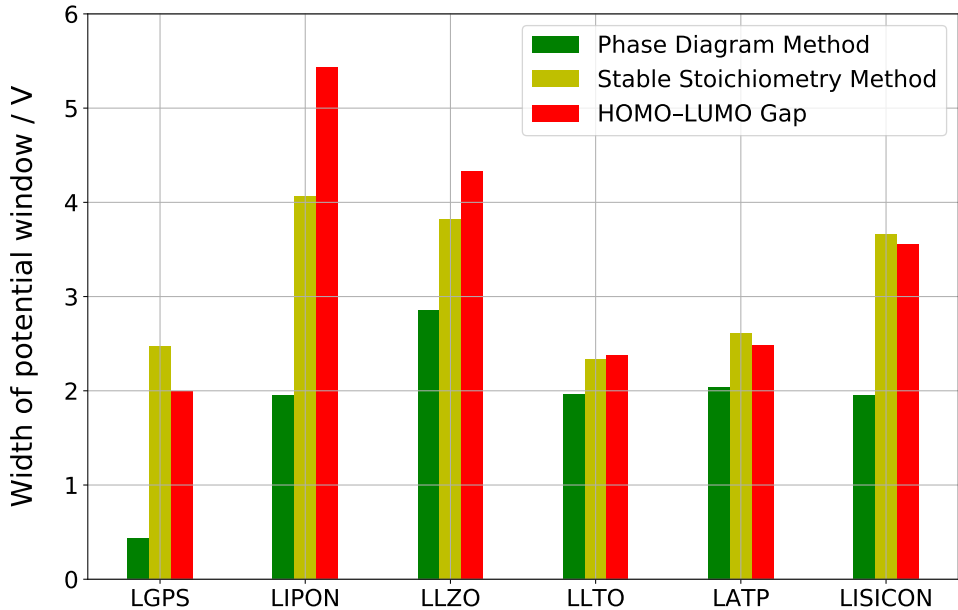


Figure 3: Width $\Delta\Phi$ of the stability potential window computed with the novel method of stable stoichiometry in comparison with the ones computed from the HOMO–LUMO band gap ΔE_{BG} and from the grand potential phase diagram method (the latter results taken from Ref³).

Connection with HOMO–LUMO method. In the following, we examine the connection between the potential window of stable stoichiometry and the electronic band gap of an SSE material. Within the HOMO–LUMO method the electronic band gap is computed in order to estimate the width of the electrochemical stability window, *vide supra*. Since only

electron exchange between the electrode and the SSE is taken into account, the electrode is assumed to be chemically inert. Therefore, the electronic band gap is generally considered to provide only an upper bound for the stability potential window of an SSE material.^{4,10}

The width of the potential window of stable stoichiometry $\Delta\Phi = \Phi_{\text{II}} - \Phi_{\text{I}} = (\Delta E_0^+ - \Delta E_0^-)/e$ is given by the energetic discontinuity in the A-chemical potential, which, as discussed in the Theory section, originates from the electronic band gap. Therefore, $e\Delta\Phi$ is expected to be approximately equal to the difference $\Delta E_{\text{F}} = E_{\text{F},\text{A}_{n+z}\text{M}} - E_{\text{F},\text{A}_n\text{M}}$ of the electronic Fermi levels of the materials A_{n+z}M and A_nM for $z > 0$. Here, we understand the Fermi level as the electronic HOMO energy and we assume purely ionic, structural terms as continuous with the A composition. For small $|z|$ the perturbation of the band structure due to variations of A-stoichiometry can be neglected and the difference of the electronic Fermi levels ΔE_{F} is approximately equal to the HOMO–LUMO band gap ΔE_{BG} of the most stable stoichiometry A_nM . Thus, the HOMO–LUMO method indirectly computes the same physical process as the novel method of stable stoichiometry, i.e. an infinitesimal exchange of A between electrode and SSE even though a chemically inert electrode is initially assumed within the HOMO–LUMO method.

However, whereas the HOMO–LUMO analysis yields estimates of the width of the stability potential window, the absolute position of the latter vs. the equilibrium potential of an A-metal anode is very difficult to be determined by electronic analysis alone, which, in turn, is enabled by the novel method of stable stoichiometry.

Thus, the insight behind the novel method provides a bridge connecting the state-of-the-art HOMO–LUMO method and grand potential phase diagram method. As discussed above, the potential window of stable stoichiometry is complementary to the stability potential window computed from the grand potential phase diagram, i.e. the former does not necessarily yield less strict potential limits than the latter, as confirmed e.g. by the results for LATP, cf. Figure 2. Due to the direct connection between the potential window of stable stoichiometry and the HOMO–LUMO band gap, the perception that the HOMO–LUMO

method yields only an upper bound for the stability potential window^{4,10} is questioned by the present analysis and results.

This general analysis is supported by the good agreement between the three quantities $\Delta\Phi$, $\Delta E_F/e$, and $\Delta E_{BG}/e$ obtained for LGPS, LLZO, LLTO, LATP, LISICON, and NASICON as presented in Table 2. Only for LIPON, a significant discrepancy was found between these three quantities. Here, ΔE_F is significantly smaller than the band gap ΔE_{BG} , because in the system with A-stoichiometry N+1 the additional electron occupies a state lying deeply within the band gap, which is not present in the band structure of the N-system. In this case, the width $\Delta\Phi$ of the potential window of stable stoichiometry lies in between the two values $\Delta E_F/e$ and $\Delta E_{BG}/e$. Figure 3 visually summarizes the widths of the stability potential window obtained from the novel method of stable stoichiometry, the HOMO–LUMO method, and the grand potential phase diagram method, the latter taken from Ref.³

Connection between SSE and electrode materials. Equations (16) and (17) appear identical to the one applied for the computation of the intercalation potential of battery electrode materials.^{31,36} However, in contrast to SSE materials, battery electrode materials must allow for an energetically continuous change in their stoichiometry and oxidation state. The A-chemical potential for such materials is almost constant in a wide range of A-stoichiometries, which results in a plateau of the equilibrium potential as a function of stoichiometry/charge as required for battery operation. For this reason, only one potential is computed for battery electrode materials. In contrast, an SSE material is operated precisely at that constant A-stoichiometry where the A-chemical potential has a discontinuous jump, which spans the potential window of stable stoichiometry and which is characterized by the computation of two potentials according to Equations (16) and (17). Consequently, the oxidation state of the SSE material remains constant during battery operation. This perspective not only provides a clear definition and distinction of an SSE material vs. a battery electrode material, but it also reveals that SSE and battery electrode materials stand in an

intimate but yet highly opposite relation with each other. Furthermore, depending on the operation potential, the same material could, in principle, serve as an SSE in one application, or as an active battery electrode material in another one, which becomes clear by rotating Figure 1 by 90° and identifying the stoichiometry change z with the stored charge.

Conclusion

We presented the potential window of stable stoichiometry as a straightforward method to characterize the electrochemical stability of solid-state electrolyte materials applied in all-solid-state batteries. If the SSE material is in its most stable stoichiometry with a formal closed shell electronic configuration, the fundamental processes of A-insertion and -extraction into/from the SSE, where A refers to the mobile species, are energetically different, because the corresponding electrons are added/extracted to/from two different energetic manifolds separated by the band gap. As a result, the A-chemical potential as a function of A-stoichiometry is discontinuous and its jump opens the potential window of stable stoichiometry. Because these processes of small SSE stoichiometry changes are not considered in state-of-the-art methods to compute the SSE electrochemical stability, the resulting stability potential windows are complementary and the overall thermodynamic stability potential window is given by their intersection. Computational results for a set of relevant Li- and Na-SSE materials reveal good agreement between the novel and state-of-the-art methods in many cases, whereas in some cases either the novel method of stable stoichiometry or the grand potential phase diagram method yielded stricter stability potential limits. Because the physical origin of the potential window of stable stoichiometry lies in the discontinuity of the A-chemical potential, which, in turn, results from the electronic band gap, the novel method represents a bridge between the HOMO–LUMO method and the grand potential phase diagram method.

Acknowledgement

This research was supported by the NCCR MARVEL, funded by the Swiss National Science Foundation. This work was supported by a grant from the Swiss National Supercomputing Centre (CSCS) under project IDs mr18 and mr28.

Supporting Information Available

The following files are available free of charge. Extended model taking into account two different classes of A-sites.

References

- (1) Peled, E. The Electrochemical Behavior of Alkali and Alkaline Earth Metals in Non-aqueous Battery Systems—The Solid Electrolyte Interphase Model. *J. Electrochem. Soc.* **1979**, *126*, 2047–2051.
- (2) Peled, E. Film forming reaction at the lithium/electrolyte interface. *Journal of Power Sources* **1983**, *9*, 253–266.
- (3) Zhu, Y.; He, X.; Mo, Y. Origin of Outstanding Stability in the Lithium Solid Electrolyte Materials: Insights from Thermodynamic Analyses Based on First-Principles Calculations. *ACS Applied Materials & Interfaces* **2015**, *7*, 23685–23693.
- (4) Lu, Z.; Ciucci, F. Metal Borohydrides as Electrolytes for Solid-State Li, Na, Mg, and Ca Batteries: A First-Principles Study. *Chemistry of Materials* **2017**, *29*, 9308–9319.
- (5) Richards, W. D.; Miara, L. J.; Wang, Y.; Kim, J. C.; Ceder, G. Interface Stability in Solid-State Batteries. *Chemistry of Materials* **2016**, *28*, 266–273.

- (6) Li, Y.; Zhou, W.; Chen, X.; Lü, X.; Cui, Z.; Xin, S.; Xue, L.; Jia, Q.; Goodenough, J. B. Mastering the interface for advanced all-solid-state lithium rechargeable batteries. *Proceedings of the National Academy of Sciences* **2016**,
- (7) Armstrong, R. The metal-solid electrolyte interphase. *Journal of Electroanalytical Chemistry and Interfacial Electrochemistry* **1974**, *52*, 413–419.
- (8) Goodenough, J. B.; Kim, Y. Challenges for Rechargeable Li Batteries. *Chemistry of Materials* **2010**, *22*, 587–603.
- (9) Ong, S. P.; Andreussi, O.; Wu, Y.; Marzari, N.; Ceder, G. Electrochemical Windows of Room-Temperature Ionic Liquids from Molecular Dynamics and Density Functional Theory Calculations. *Chemistry of Materials* **2011**, *23*, 2979–2986.
- (10) Mo, Y.; Ong, S. P.; Ceder, G. First Principles Study of the $\text{Li}_{10}\text{GeP}_2\text{S}_{12}$ Lithium Super Ionic Conductor Material. *Chemistry of Materials* **2012**, *24*, 15–17.
- (11) Ong, S. P.; Wang, L.; Kang, B.; Ceder, G. Li–Fe–P–O₂ Phase Diagram from First Principles Calculations. *Chemistry of Materials* **2008**, *20*, 1798–1807.
- (12) Sadowski, M.; Sicolo, S.; Albe, K. Defect thermodynamics and interfacial instability of crystalline $\text{Li}_4\text{P}_2\text{S}_6$. *Solid State Ionics* **2018**, *319*, 53–60.
- (13) Maier, J. Mass Transport in the Presence of Internal Defect Reactions—Concept of Conservative Ensembles: I, Chemical Diffusion in Pure Compounds. *Journal of the American Ceramic Society* **1993**, *76*, 1212–1217.
- (14) Park, H.; Jung, K.; Nezafati, M.; Kim, C.-S.; Kang, B. Sodium Ion Diffusion in Nasicon ($\text{Na}_3\text{Zr}_2\text{Si}_2\text{PO}_{12}$) Solid Electrolytes: Effects of Excess Sodium. *ACS Applied Materials & Interfaces* **2016**, *8*, 27814–27824.
- (15) Senevirathne, K.; Day, C. S.; Gross, M. D.; Lachgar, A.; Holzwarth, N. A new crystalline

- LiPON electrolyte: Synthesis, properties, and electronic structure. *Solid State Ionics* **2013**, *233*, 95–101.
- (16) Kuhn, A.; Köhler, J.; Lotsch, B. V. Single-crystal X-ray structure analysis of the superionic conductor $\text{Li}_{10}\text{GeP}_2\text{S}_{12}$. *Phys. Chem. Chem. Phys.* **2013**, *15*, 11620–11622.
- (17) Awaka, J.; Takashima, A.; Kataoka, K.; Kijima, N.; Idemoto, Y.; Akimoto, J. Crystal structure of fast lithium-ion-conducting cubic $\text{Li}_7\text{La}_3\text{Zr}_2\text{O}_{12}$. *Chemistry Letters* **2011**, *40*, 60–62.
- (18) Fourquet, J.; Duroy, H.; Crosnier-Lopez, M. Structural and Microstructural Studies of the Series $\text{La}_{2/3-x}\text{Li}_{3x1/3-2x}\text{TiO}_3$. *Journal of Solid State Chemistry* **1996**, *127*, 283 – 294.
- (19) Kothari, D. H.; Kanchan, D. Effect of doping of trivalent cations Ga^{3+} , Sc^{3+} , Y^{3+} in $\text{Li}_{1.3}\text{Al}_{0.3}\text{Ti}_{1.7}(\text{PO}_4)_3$ (LATP) system on Li^+ ion conductivity. *Physica B: Condensed Matter* **2016**, *501*, 90 – 94.
- (20) Hong, H.-P. Crystal structure and ionic conductivity of $\text{Li}_{14}\text{Zn}(\text{GeO}_4)_4$ and other new Li^+ superionic conductors. *Materials Research Bulletin* **1978**, *13*, 117 – 124.
- (21) Bijvoet, J. M.; Claassen, A.; Karssen, A. The scattering power of lithium and oxygen, determined from the diffraction-intensities of powdered lithiumoxide. *Proceedings of the Koninklijke Nederlandse Academie van Wetenschappen* **1926**, *29*, 1286–1292.
- (22) Zintl, E.; Harder, A.; Dauth, B. Gitterstruktur der Oxide, Sulfide, Selenide und Telluride des Lithiums, Natriums und Kaliums. *Zeitschrift für Elektrochemie und angewandte physikalische Chemie* **1934**, *40*, 588–593.
- (23) Kawada, I.; Isobe, M.; Okamura, F.; Watanabe, H.; Ohsumi, K.; Horiuchi, H.; Sato, T.; Ishii, T. Time-of-flight neutron diffraction study of Li_3N at high temperature. *Mineralogical Journal* **1986**, *13*, 28–33.

- (24) Brauer, G.; Zintl, E. Konstitution von Phosphiden, Arseniden, Antimoniden und Wismutiden des Lithiums, Natriums und Kaliums. *Zeitschrift fuer Physikalische Chemie, Abteilung B* **1937**, *37*, 323–352.
- (25) Ott, H. Die Strukturen von MnO, MnS, AgF, NiS, SnI₄, SrCl₂, BaF₂, Praezisionsmessungen einiger Alkalihalogenide. *Zeitschrift fuer Kristallographie, Kristallgeometrie, Kristallphysik, Kristallchemie* **1926**, *63*, 222–230.
- (26) Didisheim, J.-J.; Prince, E.; Wuensch, B. Neutron Rietveld analysis of structural changes in NASICON solid solutions Na_{1+x}Zr₂Si_xP_{3-x}O₁₂ at elevated temperatures: x=1.6 and 2.0 at 320°C. *Solid State Ionics* **1986**, *18-19*, 944 – 958.
- (27) Giannozzi, P. et al. QUANTUM ESPRESSO: a modular and open-source software project for quantum simulations of materials. *Journal of Physics: Condensed Matter* **2009**, *21*, 395502 (19pp).
- (28) Perdew, J. P.; Burke, K.; Ernzerhof, M. Generalized Gradient Approximation Made Simple. *Phys. Rev. Lett.* **1996**, *77*, 3865–3868.
- (29) Hamann, D. R. Optimized norm-conserving Vanderbilt pseudopotentials. *Phys. Rev. B* **2013**, *88*, 085117.
- (30) Schlipf, M.; Gygi, F. Optimization algorithm for the generation of ONCV pseudopotentials. *Computer Physics Communications* **2015**, *196*, 36 – 44.
- (31) Chevrier, V. L.; Ong, S. P.; Armiento, R.; Chan, M. K. Y.; Ceder, G. Hybrid density functional calculations of redox potentials and formation energies of transition metal compounds. *Phys. Rev. B* **2010**, *82*, 075122.
- (32) Kamaya, N.; Homma, K.; Yamakawa, Y.; Hirayama, M.; Kanno, R.; Yonemura, M.; Kamiyama, T.; Kato, Y.; Hama, S.; Kawamoto, K.; Mitsui, A. A lithium superionic conductor. *Nature Materials* **2011**, *10*, 682–686.

- (33) Yu, X.; Bates, J. B.; Jellison Jr., G. E.; Hart, F. X. A Stable ThinFilm Lithium Electrolyte: Lithium Phosphorus Oxynitride. *J. Electrochem. Soc.* **1997**, *144*, 524–532.
- (34) Noguchi, Y.; Kobayashi, E.; Plashnitsa, L. S.; Okada, S.; Yamaki, J.-i. Fabrication and performances of all solid-state symmetric sodium battery based on NASICON-related compounds. *Electrochimica Acta* **2013**, *101*, 59–65.
- (35) Warhus, U.; Maier, J.; Rabenau, A. Thermodynamics of NASICON ($\text{Na}_{1+x}\text{Zr}_2\text{Si}_x\text{P}_{3-x}\text{O}_{12}$). *Journal of Solid State Chemistry* **1988**, *72*, 113 – 125.
- (36) Urban, A.; Seo, D.-H.; Ceder, G. Computational understanding of Li-ion batteries. *npj Computational Materials* **2016**, *2*, 16002.